JOURNAL OF THE ROYAL SOCIETY Interface

Quantitative morphometric measurements using site selective image cytometry of intact tissue

Hyuk-Sang Kwon, Yoon Sung Nam, Dominika M Wiktor-Brown, Bevin P Engelward and Peter T.C So

J. R. Soc. Interface 2009 **6**, S45-S57
doi: 10.1098/rsif.2008.0431.focus

Interface focus

J. R. Soc. Interface (2009) **6**, S45–S57
doi:10.1098/rsif.2008.0431.focus
Published online 2 December 2008

Quantitative morphometric measurements using site selective image cytometry of intact tissue

Hyuk-Sang Kwon[1], Yoon Sung Nam[2], Dominika M. Wiktor-Brown[2], Bevin P. Engelward[2,*] and Peter T. C. So[1,2,*]

[1]*Department of Mechanical Engineering, and* [2]*Department of Biological Engineering, Massachusetts Institute of Technology, Cambridge, MA 02139, USA*

Site selective two-photon tissue image cytometry has previously been successfully applied to measure the number of rare cells in three-dimensional tissue specimens up to cubic millimetres in size. However, the extension of this approach for high-throughput quantification of cellular morphological states has not been demonstrated. In this paper, we report the use of site-selective tissue image cytometry for the study of homologous recombination (HR) events during cell division in the pancreas of transgenic mice. Since HRs are rare events, recombinant cells distribute sparsely inside the organ. A detailed measurement throughout the whole tissue is thus not practical. Instead, the site selective two-photon tissue cytometer incorporates a low magnification, wide field, one-photon imaging subsystem that rapidly identifies regions of interest containing recombinant cell clusters. Subsequently, high-resolution three-dimensional assays based on two-photon microscopy can be performed only in these regions of interest. We further show that three-dimensional morphology extraction algorithms can be used to analyse the resultant high-resolution two-photon image stacks providing information not only on the frequency and the distribution of these recombinant cell clusters and their constituent cells, but also on their morphology.

Keywords: three-dimensional image; tissue cytometry; rare cell detection

1. INTRODUCTION

1.1. Tissue image cytometry

For a large population of cells, cytometry techniques provide the potential for quantitative statistical analysis of their properties. One of the first cytometry techniques that enabled researchers to quantitatively assess large numbers of cells is flow cytometry (Kamentsky & Melamed 1967; Van Dilla *et al.* 1969; Givan 2001; Melamed 2001). Its high-throughput capacity, sensitivity and specificity have made flow cytometry a valuable technique for numerous clinical and research applications. Flow cytometry is particularly valuable when a population analysis of cellular state is required or when rare cells must be detected from a large background population (Rieseberg *et al.* 2001). However, a major limitation of flow cytometry is a lack of cellular morphological information. In addition, flow cytometry often requires fairly laborious specimen preparation procedures that may introduce experimental artefacts. Motivated by these limitations inherent in flow cytometry, image cytometry was developed (Kamentsky & Kamentsky 1991; Kamentsky *et al.* 1997; Rieseberg *et al.* 2001; Ecker & Steiner 2004). In image cytometry, a population of cells is imaged on a microscope cover-slip or other types of solid support rather than analysed in suspension (Kamentsky 2001). It shares some important characteristics with flow cytometry, such as the ability to investigate large cell populations, but image cytometry also provides important additional information. Most importantly, image cytometry has the potential to be applied to tissue sections or to whole tissues, thus giving rise to valuable information on characteristics such as intracellular protein distribution, cellular morphology and spatial relationships among cells. Today, image cytometry has been applied to a number of biology assays and it is a promising avenue for identifying new protein interaction pathways (Chen & Murphy 2006) and drug discovery strategies (Perlman *et al.* 2004; Lang *et al.* 2006; Loo *et al.* 2007). Image cytometry can be used in research or in certain clinical settings as an important quantitative aid to standard histopathological analysis (Tarnok & Gerstner 2002; Gerstner *et al.* 2004).

While image cytometry has been used extensively in the study of two-dimensional cell cultures and tissue sections, the usefulness of this technique for multi-scale analysis of three-dimensional tissue volume is

*Authors for correspondence: Department of Biological Engineering, Massachusetts Institute of Technology, Cambridge, MA 02139, USA (bevin@mit.edu; ptso@mit.edu).

One contribution of 9 to a Theme Supplement 'Quantitative fluorescence microscopy: The 1st international Theodor Förster lecture series'.

Received 1 October 2008
Accepted 11 November 2008

relatively unexplored (Gorczyca *et al.* 1997; Hendricks 2001). Importantly, three-dimensional image cytometry of intact tissues does not require that the tissue be disaggregated; there is, therefore, a much lower probability of introducing specimen preparation artefacts into the analysis. Furthermore, it is known that cell–cell, cell–tissue and cell–extracellular matrix interactions are critical factors for normal cellular physiology, and that these interactions are destroyed by disaggregating cells prior to flow cytometry and are sometimes disrupted under two-dimensional culture conditions. For example, cellular morphology, as well as gene and protein expression profiles, are drastically different between cells inside native tissues compared with the same cells grown on two-dimensional tissue culture (Powers *et al.* 2002; Hwa *et al.* 2007). In pharmaceutical development, these differences may contribute to the low success rate of drug candidates in animal models and patients.

1.2. Two-photon tissue image cytometry

Most high-resolution imaging techniques are not well suited to deep tissue imaging, owing to problems with light penetration and scattering in tissues. Standard wide field microscopy (WFM) suffers from very poor resolution and contrast when attempting to image more than several micrometres from the surface of the tissue. Confocal scanning microscopy is a technique that has shown some success in imaging intact tissue. However, in practice, the axial imaging depth for confocal microscopy is less than 40 μm for many tissue types. Moreover, phototoxicity and photobleaching are additional concerns. More recently, two-photon microscopy (TPM) has been developed, offering many advantages when imaging deep into tissues (Denk 1994; Helmchen & Denk 2005). There are several inherent advantages of TPM that make it an effective strategy for three-dimensional image cytometry. TPM offers submicrometre resolution, inherent three-dimensional sectioning, high-penetration depth, low background and low photo-toxicity. For these reasons, it is particularly well suited for imaging optically thick biological specimens. It can image into some thick tissue specimens up to a few hundred micrometres in depth. While TPM has a penetration depth of several hundred micrometres, it is still insufficient to image the full thickness of whole organs of small animals. This limitation of TPM was partially overcome by incorporating an automated microtome into a high-throughput multi-photon microscope (Ragan *et al.* 2007).

Although, TPM image acquisition is generally relatively slow, high-throughput two-photon three-dimensional tissue cytometry has been developed either based on high-speed single-focus scanning (Ragan *et al.* 2007) or based on multifocal multi-photon excitation (Kim *et al.* 2007*a*). By creating image stacks tens to hundreds of micrometres into a fixed tissue block, sectioning off the top layer, and then imaging the newly exposed section, it is possible to image through an entire *ex vivo* specimen. This method provides three-dimensional images of macroscopic volume with microscopic resolution. There is a wide range of biomedical studies that are feasible using three-dimensional tissue cytometry in fields such as neurobiology, cardiology, cancer biology and muscular disorder.

1.3. Homologous recombination in transgenic mice

Cancer is caused by the accumulation of genetic changes in cells, and mitotic homologous recombination (HR) events are an important class of mutations. To study HR *in vivo*, the fluorescent yellow direct repeat (FYDR) mice were developed. In these mice, HR at an integrated transgene can reconstitute full length enhanced yellow fluorescent protein (EYFP), thus giving rise to yellow fluorescence. This mouse model enables studies of mitotic HR events *in vivo* by analysis of tissue specimens from the transgenic FYDR mice (Hendricks *et al.* 2003). Wiktor-Brown *et al* (2006) have demonstrated that WFM imaging and flow cytometry can be used to identify recombinant cells within pancreatic tissue of FYDR mice. A recent study further applied site selective two-photon tissue image cytometry to reveal that clonal expansion as a major driver of mutation loads in the pancreas of mature animals (Wiktor-Brown *et al.* 2008).

Imaging intact tissues preserves the three-dimensional architecture of the tissue specimen and thus provides important spatial and contextual information that is otherwise lost in flow cytometry. In this report, we applied two-photon tissue image cytometery to study rare fluorescent cells that arise as a consequence of HR. Importantly, recombination at the EYFP locus is not thought to significantly alter cell behaviour. Therefore, this system allows the identification of genetically different but phenotypically normal cells, and makes it possible to monitor the frequency of such cells in animals under different conditions.

1.4. Site selective tissue cytometry

Two-photon three-dimensional tissue cytometry as described previously can be used for studying HR. However, recombinant cells in the mouse pancreas appear in widely separate, isolated clusters (foci) in the tissue (figure 1). Representation TPM data are shown below. Figure 1 shows a typical two-dimensional plane of cells in a recombinant focus. Using existing three-dimensional tissue image cytometry technique to study these sparse biological events in a large tissue volume would require excessively long data-acquisition time that could compromise the quality of the tissue and produce an excessively large dataset. These challenges motivated the development of a site selective two-photon tissue cytometer, as first described in Wiktor-Brown *et al.* (2008). The basic idea of site selective two-photon tissue cytometry is quite simple. If the locations of the sparse cell clusters can be identified using low magnification WFM, automated specimen positioning will allow us to relocate these regions of interest with sufficient accuracy for subsequent high-resolution two-photon three-dimensional imaging. This three-dimensional site-selective tissue cytometer offers the best combination of experimental efficiency and

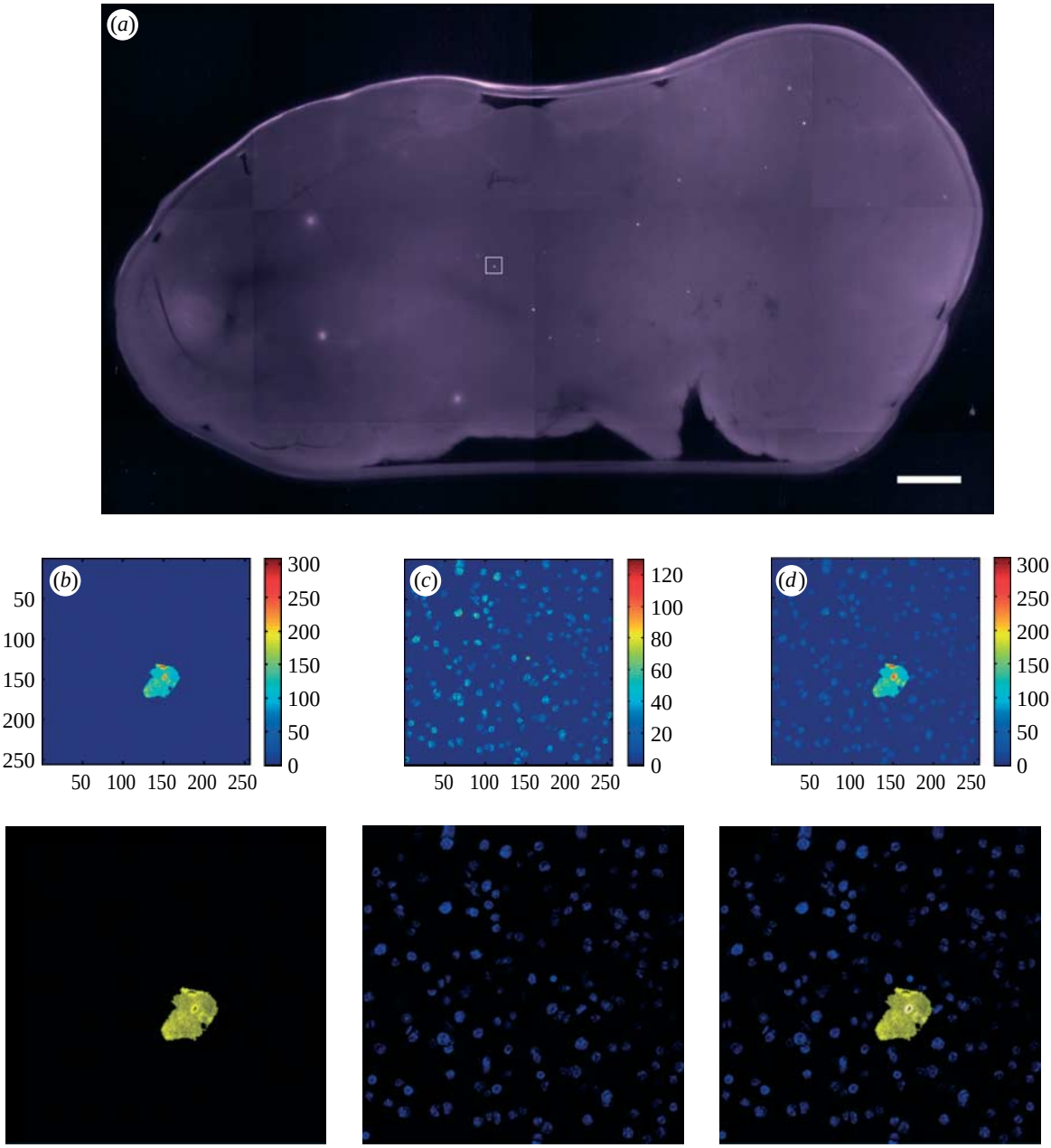

Figure 1. (*a*) Typical WFM image and two-dimensional TPM image of mouse pancreatic tissue. Typical WFM by uniform illumination of continuous wave laser was done on mouse pancreas tissue. Fluorescence recombinant foci are identified and their *x*–*y* coordinates are mapped within the composite images. Smaller WFM images (5 mm by 4 mm) were stitched to cover the whole surface of the pancreas. White scale bar indicates 1 mm. Two-photon images are composed of two-channel images from the identical FOV. TPM image is pseudo colour images with intensity. (*b*) The Green Channel has a EYFP cell cluster (*c*) image and Blue Channel has cell nuclei images. By overlaying two features (*d*), we can identify the number of cells in the cell cluster.

information content for the study of rare biological events in tissues, allowing specimens to be studied spanning four orders of magnitude in length-scale. Using this site selective approach offers significant advantages over traditional TPM. More specifically, since HR at specific locus is a rare event, the frequency of recombinant cells in the pancreas is approximately five cells per million (Wiktor-Brown *et al.* 2006). The pancreas of adult mouse contains approximately 3×10^7 cells (Taga *et al.* 1998) and has a size of approximately 2 cm by 1 cm by 0.05 cm when it was placed on a slide glass. If there were approximately 50 recombinant foci in one pancreas, it would take approximately 8.5 days (210 hours) for a typical, non-video-rate, TPM to image an entire pancreas, assuming this microscope can cover a field of view (FOV) of $240\times240\ \mu m^2$ at one frame s^{-1}. However, using three-dimensional site-selective tissue cytometry, the location of these foci can be first recorded rapidly with WFM, and then each focus can be analysed using slower three-dimensional high-resolution imaging of the foci with TPM. The estimated time for imaging all the foci using the site selective tissue cytometer is approximately 6 hours, almost an order of magnitude reduction in data acquisition time. Using the site-selective approach, acceptable experimental throughput rate can be achieved using a standard TPM without video rate capability. Furthermore, wide-field, low magnification imaging also provides a

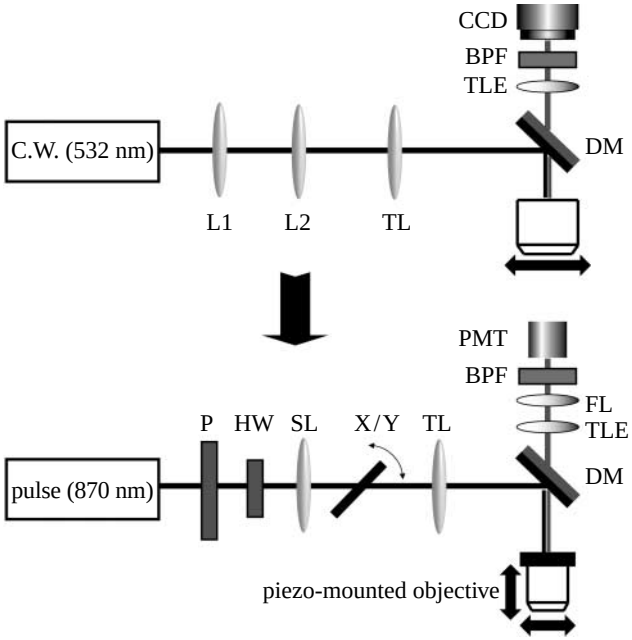

Figure 2. Optical layout for three-dimensional site-selective tissue cytometry. Black line indicates the excitation beam and Gray line indicates the emission beam. C.W. (532 nm) denotes the excitation source for WFM; continuous wave diode laser with 532 nm wavelength. L1 and L2 are combination of lenses for magnifying and collimating the excitation laser beam. DM denotes dichroic mirror. TLE denotes emission tube lens inside microscope body. BPF denotes band pass filter in emission path. CCD denotes for the charge-coupled device. Pulse (870 nm) denotes the excitation source for TPM. P denotes the polarizer. HW denotes half wave plate. With these polarization and power level can be adjusted. SL denotes scan lens. X/Y denotes x–y mirror scanner. TL denotes tube lens for excitation path. FL denotes de-scanning lens. Horizontal/vertical arrow indicates the motion of the x–y specimen stage.

useful record of the global tissue histological state as a background for the high-resolution two-photon three-dimensional images. Although, the use of site selective two-photon cytometry in the quantification of mutation load during ageing has been demonstrated in our previous publication (Wiktor-Brown *et al.* 2008), the detailed hardware design and the software algorithms for image processing remain to be fully described. This report will focus on the hardware and software design of this site selective two-photon tissue image cytometer. Previous two-photon tissue image cytometry studies have focused only on the detection and the counting of rare cells (Kim *et al.* 2007*b*; Wiktor-Brown *et al.* 2008). The high-resolution image information contained within the three-dimensional image stacks has not been fully explored to extract cytometric information from these rare cell clusters and their constituent cells. In this report, we demonstrated that high-throughput quantification of the three-dimensional morphology profiles of these recombinant cells and their cell clusters is possible.

2. MATERIALS AND METHODS

2.1. Preparation of FYDR mouse specimen

Two female 70 week old FYDR mice and seven female four week old FYDR mice were studied to quantify the distribution and morphology of recombinant cells in the pancreas. Each mouse was given food and water ad libitum. In order to visualize nuclei in isolated tissues, the mouse was given a single retro-orbital injection of 0.04 mg Hoechst in sterile phosphate buffered saline (PBS, pH 7) per gram of mouse body weight 20 min prior to humane sacrifice. Intact pancreata were isolated, rinsed and soaked in ice cold PBS (pH 7.4) containing 0.01 per cent soya bean trypsin inhibitor (Sigma). The pancreas is relatively soft and can be readily moulded to fit the specimen holder. Pancreatic tissue was uniformly compressed between two coverslips separated by 0.5 mm spacers.

2.2. Site selective two-photon tissue cytometry

Both WFM and TPM are common techniques that can be readily implemented. The optical layout for both systems is shown in figure 2. There are many common elements for both imaging modalities. The core of the instrument is a Zeiss microscope (Axiovert 110, Zeiss Thornwood, NY). An automated x–y stage (H101, Prior Scientific, Rockland, MA) was used to translate the specimen under the objective. For data acquisition, the data acquisition computer was equipped with a custom made data acquisition card and software. These customized tools were applied both to TPM as well as to running Viewfinder software (Pixera Corporation, San Jose, CA) for WFM. The selection between WFM and TPM modes requires a manual exchange of objectives as well as manually directed excitation light manipulative through various optical paths via several switchable mirrors.

2.2.1. Wide-field fluorescence microscopy. Although WFM is limited in terms of high-resolution deep tissue imaging, it is an effective method for evaluating a wide FOV, which is particularly useful for identifying rare

objects within a relatively large organ. Although WFM images of these rare objects are blurred, their locations can be mapped even through millimetre thick tissue provided that the objects are sufficiently fluorescent. For WFM, the light beam from a green diode laser (BTG—2S, Beam of Light Technologies, Clackamas and Oregon) is expanded and focused at the back focal plane of a low magnification, low NA, objective (1.25X Plan Apo, 0.04 NA, Olympus, Center Valley, PA) resulting in a collimated beam uniformly illuminating the specimen. The beam expansion unit controlled the size of FOV. A Pixera Pro 150ESM Pander system was used that featured a monochrome CCD sensor with 1.5 M pixels, 62 dB signal-to-noise ratio, low dark noise and detection sensitivity of 0.01 lux. This WFM system has a FOV of 4.7 mm by 6 mm. The resolution for WFM is 8 μm (corresponding to $0.61\lambda/\mathrm{NA}$) with 532 nm excitation wavelength. The time required for imaging these pancreas specimens with adequate signal to noise ratio (SNR) using WFM is approximately 10 s per frame. Typically, five frames are averaged. Since the whole pancreas specimen is bigger than a single FOV, a series of WFM images were montage together using an automated x–y stage. To accurately stitch these images together, images were taken such that they have 1 mm overlap along x-direction and 0.67 mm overlap along y direction. After the composite image is formed, the location of each focus was identified and recorded in order to guide subsequent high-resolution TPM imaging.

2.2.2. Two-photon fluorescence microscopy. The TPM system employed consisted of a femtosecond Ti : Sapphire laser, powered by a continuous wave diode pump laser, (Tsunami, Spectra Physics, Palo Alto, CA). A half wave plate (CVI Laser, Inc., Putnam, Connecticut) and a Glan-Thomson polarizer were used to control the excitation power; the maximum excitation power was set to avoid excitation saturation of chromophores or specimen photodamage. The average laser power incident upon the specimen was less than approximately 20 mW. This experiment utilized a non-video-rate two-photon system, although even higher throughput can be achieved using video rate two-photon image cytometers described previously (Kim *et al.* 2007*b*; Ragan *et al.* 2007). The laser beam was raster scanned across the sample plane by 500 Hz bandwidth x–y scanner mirrors (Cambridge Technology, Cambridge, MA). The laser beam was coupled into an inverted microscope by means of a modified epi-luminescence light path. The beam was reflected by the dichroic mirror towards the objective and was focused on the specimen. The objective was used to focus the laser light onto the sample and directed the fluorescent signal to the emission path of the microscope. A 20X, 0.75 NA objective with a working distance of 0.6 mm (Zeiss, Fluar, Thornwood, NY) was chosen for this application. This choice is a compromise between resolution and FOV. A typical image consisted of 256×256 pixels. The FOV was approximately $240\times240\ \mu\mathrm{m}^2$, allowing most of the typical recombination foci in the pancreas to be imaged in their entirety in one frame, and thus eliminating the need to montage multiple FOVs. Signal photons were collected using a photomultiplier tube (R7400, Hamamatsu, Bridgewater, NJ) detectors. To perform three-dimensional volume scans, the objective was mounted on a computer-controlled piezoelectric objective translator (MIPOS 500, Piezosystem Jena, Jena, Germany). The maximum z-axis travel range was 300 μm. Axial translation of the objective yielded a z-stack of image planes. Typically, approximately 50 layers were imaged at 1 μm depth increment for each focus. This depth range was chosen so that three-dimensional reconstruction using two-dimensional TPM image stack would cover approximately 3–4 layers of cells spanning the full thickness of typical clusters of fluorescent recombinant cells.

In addition to EYFP, Hoechst was further used as nucleic stain allowing EYFP cells in the clusters to be distinguished and counted. Both Hoechst and EYFP were simultaneously excited at 870 nm and their emissions were collected at the corresponding PMT channels. The TPM data acquisition time for an image was approximately 7 s per frame using a pixel clock rate of 10 kHz. Two detector channels were implemented by using a dichroic mirror and two band-pass filters (Chroma Technologies, Brattleboro, VT). The emission filter used for detecting Hoechst stained nuclei in the Blue Channel is centred at 470 nm with a pass band of 40 nm covering the emission maxima of Hoechest at 483 nm. The emission filter for detecting EYFP in the Green Channel is centred at 530 nm with a pass band of 40 nm which is effective for EYFP with its emission maxima at approximately 527 nm. The current signals from the PMTs were converted to single photon counts via a custom designed transimpedience/discriminator circuitry and recorded by the data acquisition computer (Buehler *et al.* 2005). Images are generated by temporally correlating the detected signal stream with the known raster-scanning pattern of the scanners.

Intensity loss due to photobleaching was estimated by imaging the same EYFP focus over time. There was little change within 24 hours after harvest of the pancreas tissue specimen at the power level used.

2.2.3. Imaging procedures using site-selective tissue cytometry. The first step in the imaging procedure is to align the FOV for both imaging modalities. Each objective has a different FOV. The centres in the FOVs for both imaging modalities were identified, and accurately aligned by imaging a standard specimen slide containing a known distribution of fluorescent polystyrene spheres. Any remaining difference in FOV centres is noted, recorded and accounted for in specimen stage positioning. After the alignment process, the flatness of the FOV was assessed by imaging a fluorescein isothiocyanate solution. Slight non-uniformity in the field is unimportant and can be corrected digitally by normalizing subsequent images using the information contained in the fluorescein solution image.

For imaging the FYDR mouse pancreas, the specimen was placed on a slide glass and affixed to a robotic x–y stage. The specimen was imaged first by WFM using the low magnification, 1.25X objective.

The robotic stage raster was used to scan the specimen allowing the whole specimen to be imaged. The WFM images were subsequently stitched together, examined and used for locating rare recombination foci. All possible candidate sites were identified, verified by eye and their locations recorded. High-resolution two photon imaging was then performed at the corresponding regions of interest, providing a series of image stacks, each representing a single focus in the pancreas.

2.3. Image processing and analysis

The TPM image stacks of pancreatic tissue were comprised sequential two-dimensional images with 1 µm incremental steps along the axial direction. The image stacks further contained two colour channels of information from the identical FOVs. The Blue Channel contained images of the cell nuclei, while both the EYFP expressing cells and the nuclei were visible in the Green Channel. All of image analysis algorithms were written in MATLAB (MathWorks, Natick, MA), with its accompanying image processing toolbox.

2.3.1. Image pre-processing. Typical microscope tissue images have various defects, such as hot spots, that should be removed or minimized with pre-processing routines. Since the average intensity of an object in these images was only tens to hundreds of photon counts and shot noise was the dominating factor in these images. Additional noise may originate from the detector and its electronics, specimen auto-fluorescence and environments such as light leakage from peripheral electronic equipments. Owing to the emission spectrum of the dye, there was spectral bleed-through from Blue Channel nuclei signal into the Green Channel and were corrected by linear spectral decomposition. Second, an intensity threshold was set to remove background noise and to improve the image SNR. This threshold was set by taking a background image in tissue with no EYFP expression, and setting the intensity threshold to a level that was 10 per cent higher than the measured background signal. This threshold values were held constant throughout the experiment.

2.3.2. Image segmentation. In this study, we need to segment two structures: the EYFP cell clusters and the nuclei (figure 3). Segmentation was performed on each two-dimensional image of a three-dimensional stack (figure 4).

For widely separated EYFP cell cluster, their boundaries were determined in the Green Channel images by applying a simple global intensity threshold. From this binary threshold image, a segmented image was produced by associating pixels that were corresponding to the same clusters. The association of a pixel to a particular cell cluster was done by examining its connectivity. First, each eight-way connected set of pixels was marked as a distinct region of its own. Second, each connected group of pixels, corresponding to a distinct cell cluster, was further assigned a unique integer value as a label.

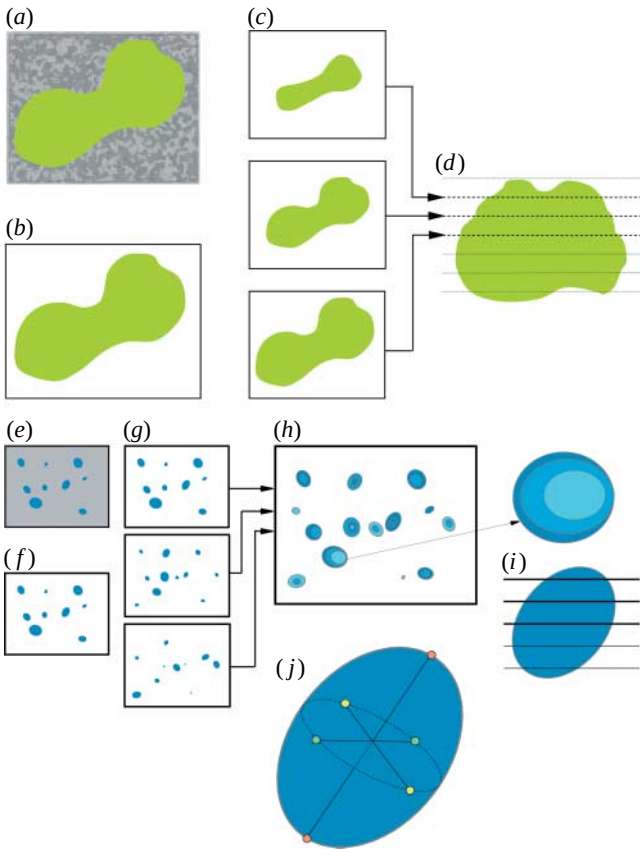

Figure 3. Imaging process procedure for obtaining three-dimensional EYFP cell clusters at one isolated focus site, and identifying three-dimensional nucleus. Raw images (*a*,*e*; image acquired) contain noise which was removed by filtering and setting the threshold. Using these noise-free images (*b*,*f*; noise reduction) obtained at different depth, segmentation was done using two-dimensional segmentation algorithm. By carefully connecting by checking overlaps between adjacent two-dimensional EYFP segmented images, three-dimensional EYFP cell cluster (*d*) is constructed. In two-dimensional segmentation on nucleus, an additional operation such as applying watershed algorithm was applied in order to discriminate possibly clustered nuclei (*g*). Then the two-dimensional segmented images of a nucleus in adjacent planes were connected (*h*) in terms of checking overlap and distances (between centroids), and realized as a three-dimensional nucleus. Various calculations can be done with this nucleus in three-dimensional using pixel and intensity information (*j*).

The nuclei can be in close proximity. Although, more advanced three-dimensional nuclear segmentation algorithms have been developed (Al-Kofahi *et al.* 2008; Bjornsson *et al.* 2008), we found that the segmentation of these nuclei is successful for this dataset with a simple approach consisting of an intensity-based threshold followed by a watershed algorithm on the Blue Channel images. After applying a global intensity threshold, a watershed algorithm was further applied to break apart regions that contain closely adjacent nuclei (Castleman 1998). To ensure the robustness of the watershed step, it was necessary to smooth the region boundaries by removing high-frequency noise in the image. A two-dimensional Gaussian filter was applied to the image prior to the

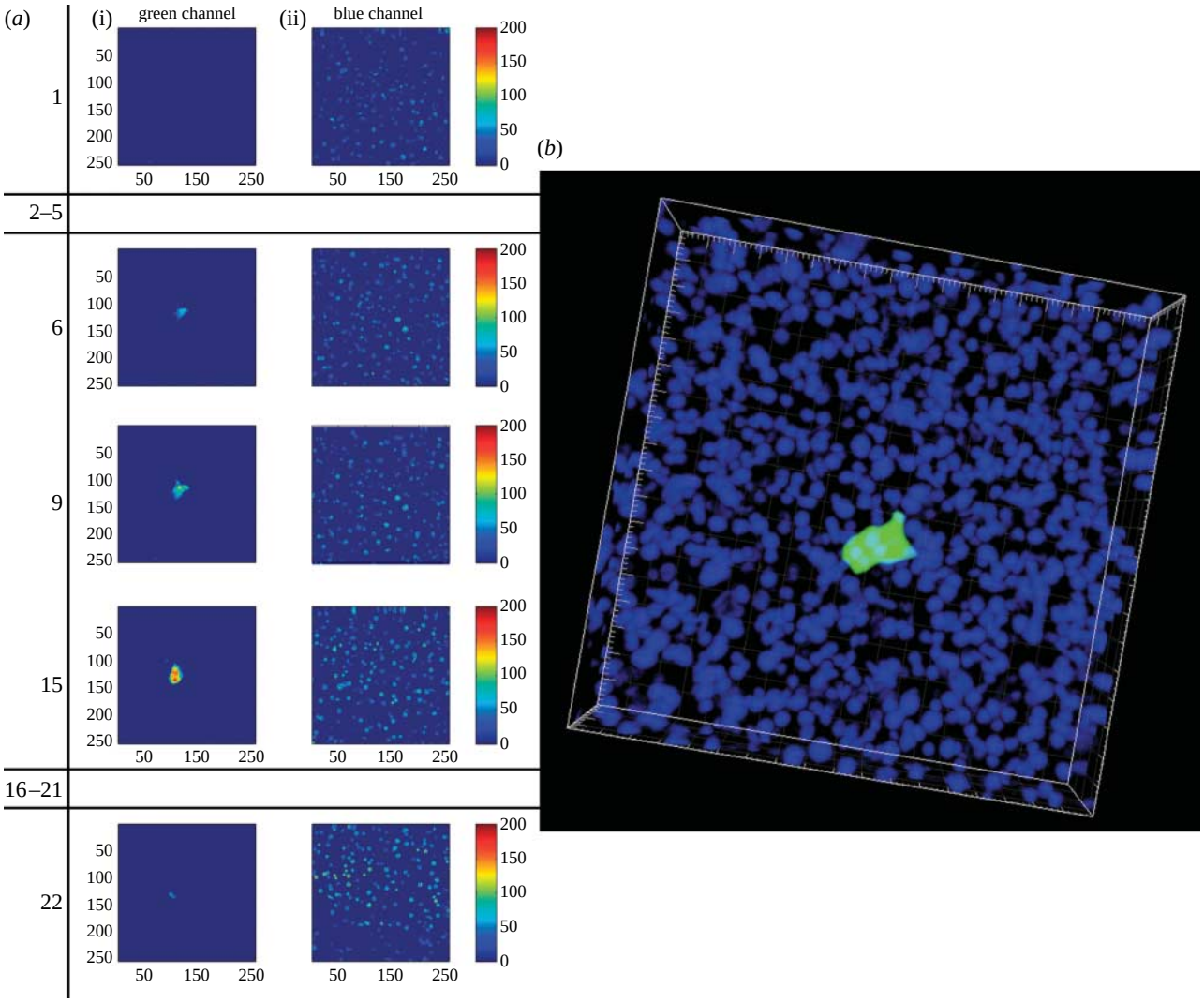

Figure 4. Three-dimensional reconstruction of nuclei and EYFP cell cluster from TPM images of mouse pancreatic tissue. (*a*(i) *Green Channel*, (ii) *Blue Channel*) TPM images were taken at 870 nm with 50 ml deep with 1 ml incremental step. FOV is 240 by 240 ml. By stacking two-dimensional images, (*b*) three-dimensional volume image was generated. There are seven cells in the EYFP recombinant cell cluster.

application of the watershed algorithm. After segmentation, individual regions corresponding to the nuclei were labelled as described before.

All the previous image processing steps were done on two-dimensional images. After successful segmentation of both the nuclei and the foci in two dimensions, the connectivity of these objects in three dimensions was established. Individual nuclei were reconstructed and identified in three dimensions by connecting two-dimensional nucleus segmentation through a three-dimensional image stack. This procedure was done in two steps. First, pixel connections were checked. Connectivity was assumed if any part of a two-dimensional nucleus was overlapping in terms of its lateral coordinate with another two-dimensional nucleus on an adjacent plane. From this, the entire set of two-dimensional segments comprising the same nucleus was identified. Second, the two adjacent two-dimensional nucleus segments in the different z-plane were checked by the distance of their centroids. The typical size of the nucleus in this tissue is approximately 10–15 μm. We require that the centroids of adjacent planes to be within 5 μm to be considered truly connected and counted as a single nucleus. For labelling, each centroid at each plane was checked first, and if it was associated with a centroid from a previous plane, it was identified as the same nucleus. If a centroid had no associations from the previous plane, it was labelled as a different nucleus. All the nuclei in three dimensions were identified and labelled by this manner. The reconstruction of EYFP foci in three dimensions was done similarly.

2.3.3. Morphological quantification. After segmentation and labelling, we were ready to assess the morphology of the nuclei, foci and their relative spatial distribution. Quantitative data were collected for seven parameters: (i) the total number of nuclei inside of each recombinant EYFP focus, (ii) the size of each EYFP focus, (iii) the intensity of each EYFP focus, (iv) the shape of each EYFP focus, (v) the size of each nucleus, (vi) the intensity of each nucleus, and (vii) the shapes of the nuclei (ellipticity).

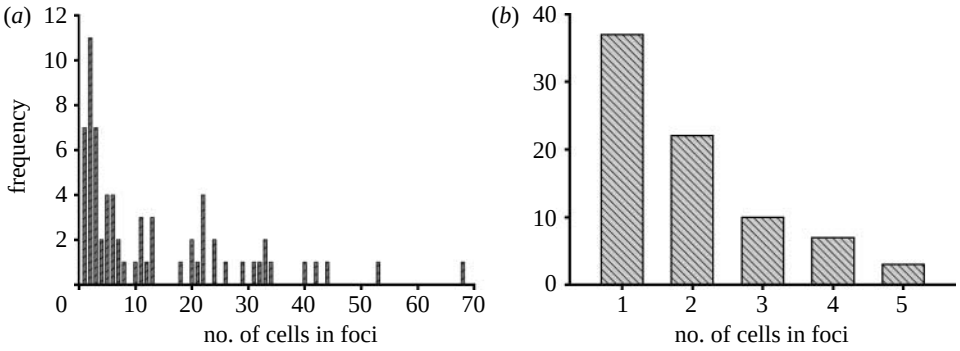

Figure 5. (*a*,*b*) Frequency histogram. The frequency versus number of cells inside each recombinant EYFP foci was plotted for each case.

3. RESULTS AND DISCUSSION

3.1. Visualization of recombinant foci in three dimensions

After spectral separation, the EYFP and nuclei at different depths are shown in figure 4. By combining these two-dimensional images at discrete planes with 1 μm incremental steps in *z*, three-dimensional reconstruction of the recombinant EYFP focus and nuclei was accomplished using commercially available Imaris v. 5.0 software.

3.2. Quantification of recombination events in the two mouse age groups

TPM images were acquired and analysed to characterize fluorescent recombinant cell clusters in a mouse pancreas. We imaged 79 foci in the pancreas of seven mice that were four weeks old. The number of cells inside of each EYFP cell cluster for this juvenile mouse group was found to vary from 1 to 5. We also imaged 68 foci using two mice that were more than 70 weeks old. The number of cells inside the EYFP cell clusters for this aged mouse group varied from 1 to 68. The number of cells within the EYFP cell clusters for each of the two age groups is shown in figure 5 as previously published (Wiktor-Brown *et al.* 2008). It was noted that only 10 per cent of the recombinant foci in the aged mice were comprised a single cell, whereas 47 per cent were observed in the young animals. Since, it is expected that recombinant cells will divide, as the animals age, the presence of single cell foci in the aged animals are consistent with the hypothesis that de novo recombination events occur throughout the lives of the animals. Of the foci analysed in pancreatic tissue of juvenile mice, the largest recombinant focus contained five cells. By contrast, approximately 40 per cent of recombinant EYFP foci in aged mice contain more than five cells, with one focus containing 68 cells. Overall, from juvenile to aged mice, the median number of cells per focus increases from two to six cells.

The size of each EYFP cell cluster was measured in terms of its vertical height with respect to the image plane. The height of EYFP cell clusters increased with the number of cells inside focus as shown in figure 6. The distributions of the heights of EYFP cell clusters for juvenile and aged mice are clearly continuous but far from normal. The two-sided Wilcoxon rank-sum test (Siegel 1956) will be used here, and in the reminder of this section, to determine if the means of the distribution are the same. Median heights were found to be 31 and 18 μm for aged and juvenile, respectively. Using a 5 per cent significance level, the Wilcoxon test returns a *p*-value of 0.90 indicating that the means cannot be distinguished. Clearly, the clusters in aged mice have larger height than juvenile mice as expected. The slope of the fit measures the rate of cluster thickness increasing with the number of cells contained within this cluster. The measured slope is 2.6 and 2.3 μm per cell for aged and juvenile mice. These values characterize the relative horizontal spread (parallel to organ surface) versus vertical spread (perpendicular to organ surface) of the recombinant cell clusters and they appear to be similar for both age groups. The size of the EYFP cell cluster was also measured in terms of its volume. The volume of EYFP cell clusters increases as the number of cells inside foci increases as shown in figure 7. The median volumes per cell for aged and juvenile mice are found to be 3070 and 3005 μm^3, respectively. A *p*-value of 0.59 indicates that the cell volume is indistinguishable between the age groups. Assuming spherical cells, their radii were found from the volume data as 10 ± 4 and 10 ± 4 μm for aged and juvenile, respectively. This radius is much larger than the rate of cluster height increase per cell indicating that clusters spread predominately parallel to the organ surface rather than spherically.

The brightness of each EYFP focus was also measured in terms of average value of intensity per cell. Figure 8 shows that the brightness of EYFP did not vary with focus size, as expected. The median values for aged and young mice are found to be 3.1×10^5 [AU] and 2.0×10^5 [AU], respectively. The *p*-value obtained is 0.9 indicating that the brightness values of recombinant cells in juvenile and aged mice are not distinguishable.

To learn more about possible morphometric differences among foci, the size of each nucleus was measured. The volume of the nucleus appears to be independent of focus size, as shown in figure 9. Median values are found to be 236 and 161 μm^3 for aged and juvenile, respectively, with a *p*-value of 0.90 from Wilcoxon rank-sum test indicating that nuclei sizes are similar for mice of both age groups. The lengths of three

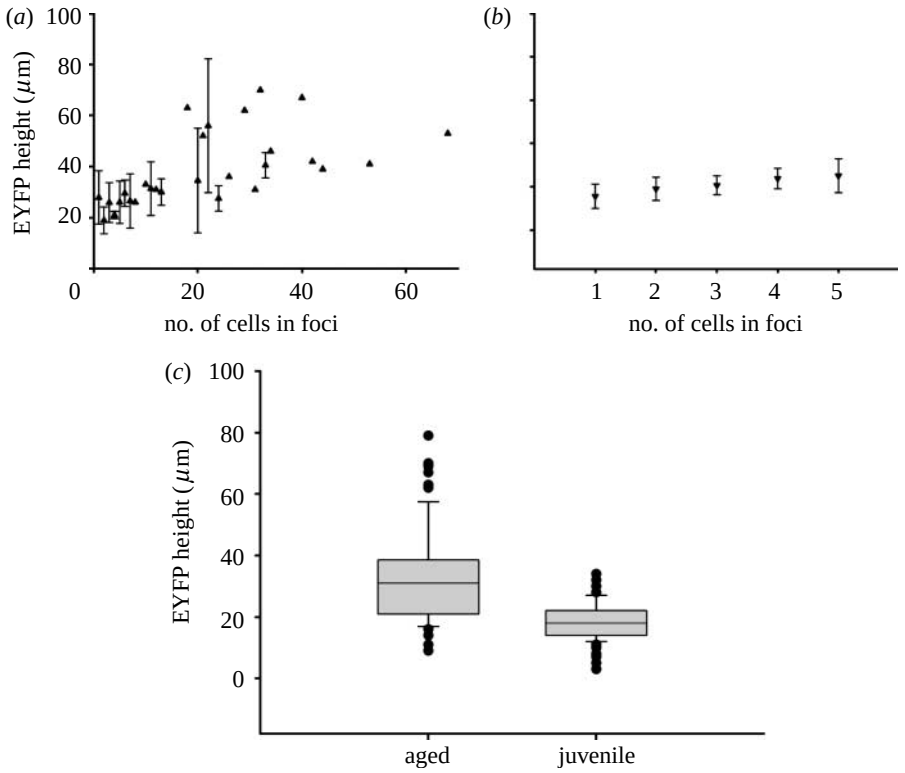

Figure 6. EYFP cell cluster height. EYFP cell cluster height versus number of cells inside of recombinant EYFP foci was plotted. The data point in (*a*,*b*) represents the average value with error bar if available. The box plot (*c*) has lines at the lower quartile, median and upper quartile values.

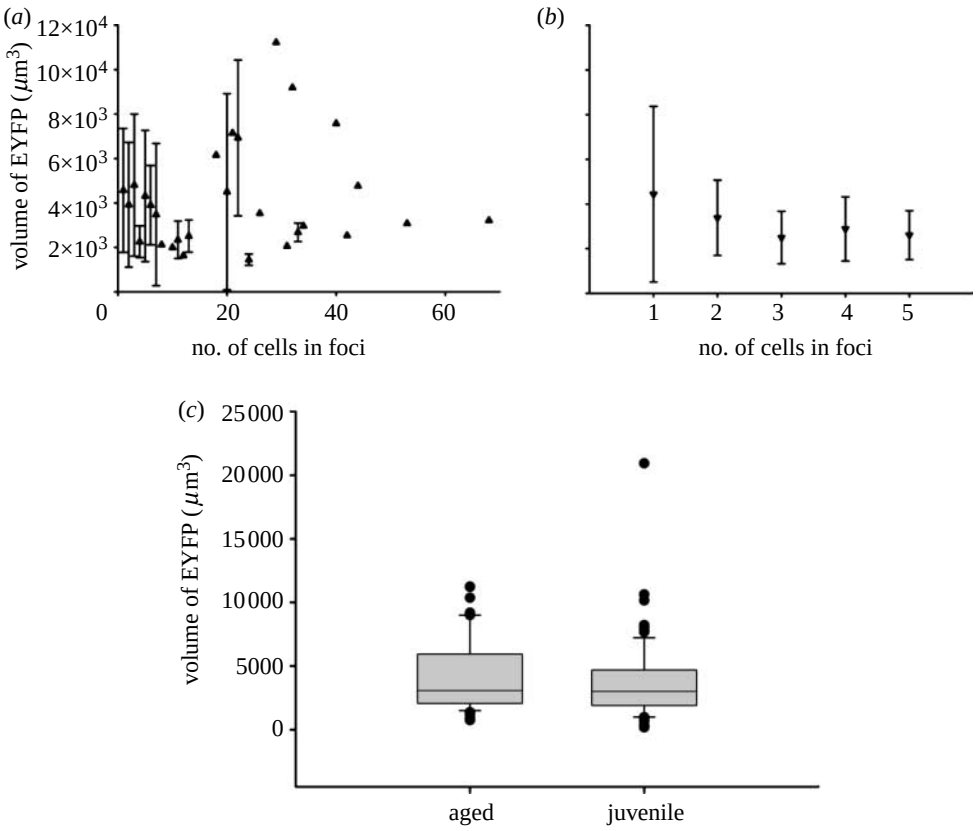

Figure 7. Volume of EYFP cell cluster per nucleus versus number of cells inside of recombinant EYFP foci was plotted. The data point in (*a*,*b*) represents the average value with error bar if available. The box plot (*c*) has lines at the lower quartile, median and upper quartile values.

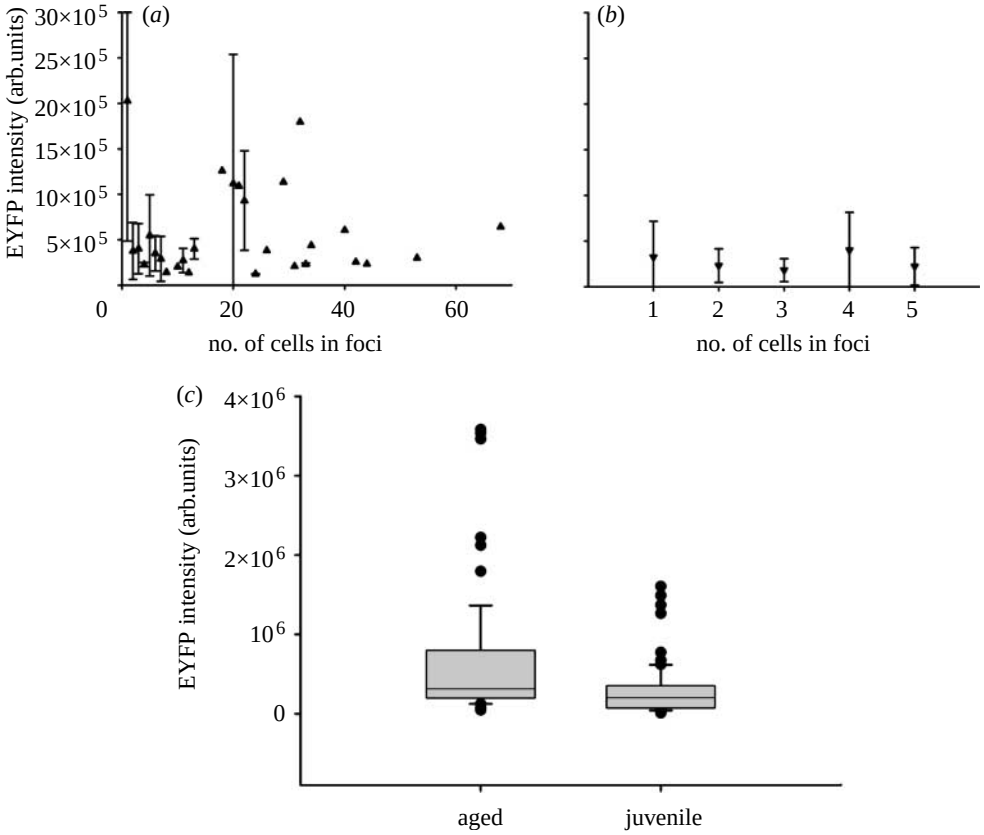

Figure 8. EYFP cell cluster brightness per cell versus number of cells in recombinant EYFP foci was plotted. The data point in (*a*,*b*) represents the average value with error bar if available. The boxplot (*c*) has lines at the lower quartile, median and upper quartile values.

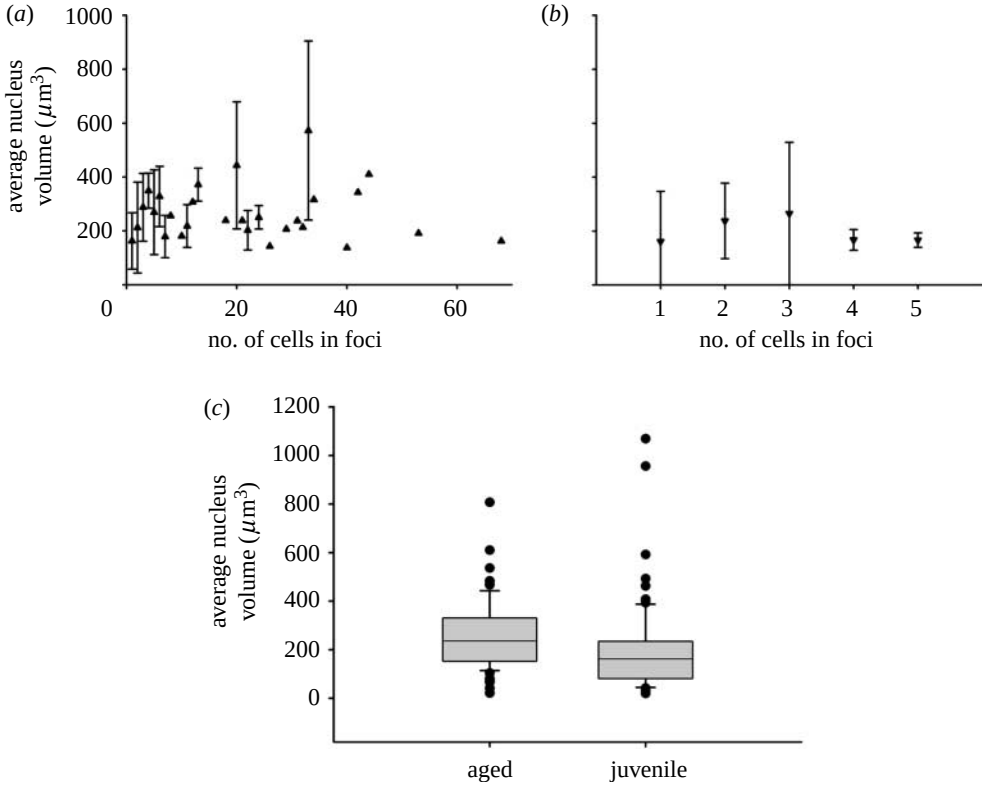

Figure 9. Volume of nucleus versus number of cells in recombinant EYFP foci was plotted. The data point in (*a*,*b*) represents the average value with error bar if available. The boxplot (*c*) has lines at the lower quartile, median and upper quartile values.

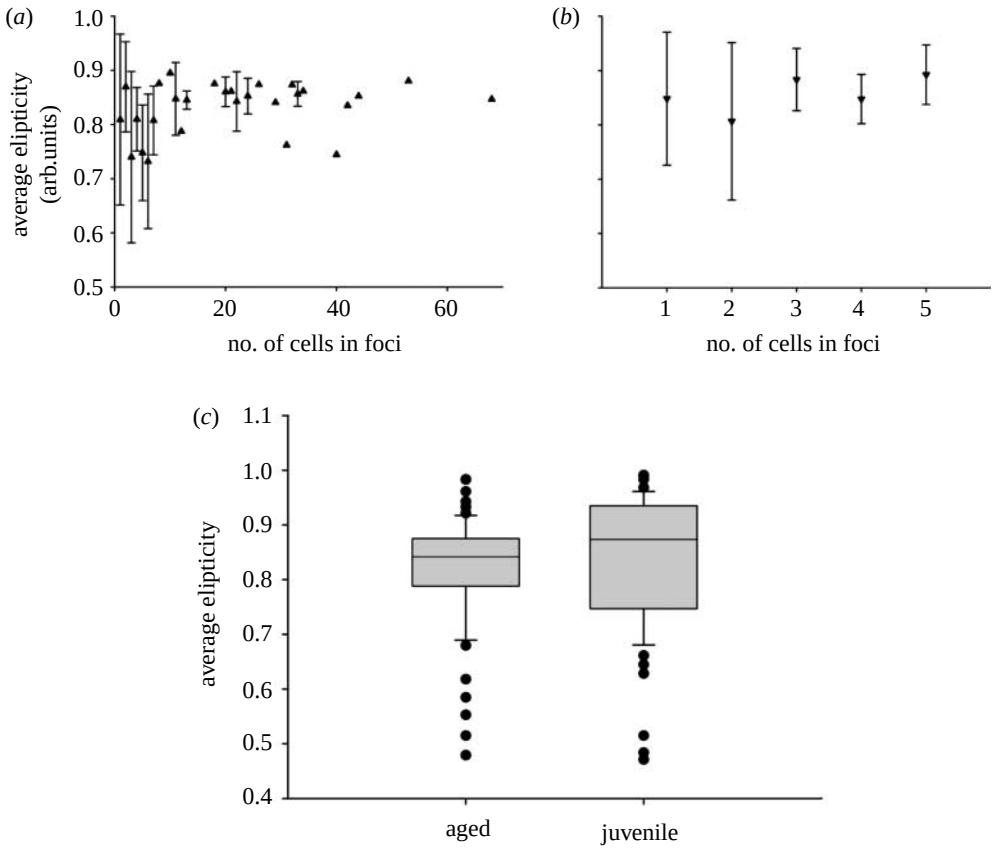

Figure 10. Elipticity of nucleus was found using the biggest and smallest values of major lengths. The data point in (*a*,*b*) represents the average value with error bar if available. The boxplot (*c*) has lines at the lower quartile, median and upper quartile values.

principal axes were computed for each nucleus at each EYFP focus. From these lengths, we can compute the elipticity of the nucleus. Median elipticity values are 0.84 and 0.87 for aged and juvenile, respectively (figure 10). Comparing the two measurements, the *p*-value is 0.96 indicating that the nuclei have comparable elipticity.

The consistency of cell EYFP expression levels, cell volume, nuclei size and nuclear elipticity among foci size are consistent with the possibility that they contain the same cell type, independently of their size. Furthermore, the observation that the morphological parameters of the cells fall into a single cluster, regardless of the size of the foci, is consistent with the possibility that cell clusters comprised a single-cell type. Previous studies in which yellow fluorescent cells were analysed by immunohistochemistry showed that the majority of cells within foci are acinar cells (Wiktor-Brown *et al.* 2008). Here, we observed that the size and shape of cells within recombinant cell foci are consistent with the morphology of acinar cells, and provides further evidence that there is little differentiation of cells into different cell types during clonal expansion.

We further calculate the nuclear density in the young and old mice. All of the three-dimensional TPM image stacks were used to find the number of cells per unit volume. This was done by counting the total number of nuclei. Using the size of both FOV and number of *z*-planes, each nucleus density can be calculated. It was found that there are 31 ± 5, and 30 ± 3 (the uncertainty here are standard deviations) cells in a specified volume of 57 600 μm^3 for juvenile and aged cases, respectively. There are no obvious changes in the number of cells per unit volume with age. Based on this information, we can conclude that recombinant foci share similar morphology compared with the rest of the pancreas.

Flow cytometry provides an alternative approach to estimate the frequency of rare fluorescent recombinant cells. Here, we compared the results obtained with flow cytometry and TPM tissue cytometry systems to evaluate the relative sensitivity of these methods for detecting rare fluorescent cells. FC has a capability of detecting over 100 000 cell min^{-1}. Regular TPM has a rate of 1800 cells min^{-1}. However, site-selective three-dimensional cytometry based on TPM can be used for imaging whole organ pancreatic tissue in 6 hours assuming that there are 50 recombinant foci. The total volume of the pancreas tissue was approximated by multiplying the surface area found from WFM with the known spacer thickness (500 μm; table 1). The surface area was approximated by drawing a curve along the boundary of the pancreas tissue using commercially available ImageJ commands (free hand selections + analyse/measure). The total number of cells was found for each pancreas tissue. Total number of cells was approximated by total volume times and the number of cells per unit volume. Using the information of the number of recombinant cell, and total number of cells in pancreas tissue, a frequency plot was generated (figure 11).

The mean number of recombinant cells in pancreatic tissue was found to be equal to 2.8 and 2.0, respectively. The Wilcoxon rank-sum test returns a

Table 1. Physical characteristics of FYDR mice pancreatic tissue. (Total volume and total cell of pancreas tissue of juvenile mice ($n=7$) and aged mice ($n=2$) were measured. Total number of recombinant cells was found from TPM images. Ratio of total number of recombinant cells to total number of cell was computed.)

	total volume (mm^3)	total number of cells	total number of recombinant cells	ratio ($1 : 10^6$ cells)
juvenile 1	55.7	30 093 472	38	5
juvenile 2	61.7	33 335 139	25	3
juvenile 3	52.275	28 243 021	7	1
juvenile 4	66.695	36 033 826	20	2
juvenile 5	61.795	33 386 465	20	2
juvenile 6	49.33	26 651 903	32	5
juvenile 7	48.12	25 998 167	12	2
aged 1	116	60 748 636	649	43
aged 2	105	52 631 361	249	19

p-value of 0.87 indicating that flow cytometry and image cytometry returns comparable results in terms of cell counting. While flow cytometry is more efficient, image cytometry can provide additional cellular morphological information.

4. CONCLUSIONS

Here, we have described novel approaches for high-throughput site-selective cytometry to study clonal expansion of cells within intact tissue. In a previous study, we demonstrated that the number of recombinant cells can be measured in FYDR mice; in this study, we show that quantitative morphological analysis of these recombinant cells and their clusters can also be performed. Importantly, these methods are some of the first permitting quantitative analysis over a size scale spanning four orders of magnitudes. We apply this powerful approach for the rapid detection of rare fluorescent cell clusters throughout the entire organ over centimetre length-scales while quantifying the three-dimensional morphology of each fluorescent cell clusters and their constituents' cells on the micrometre scale. The frequency, brightness and the sizes of the both recombinant foci and nuclei inside the clusters have been quantified.

In three-dimensional site-selective tissue cytometry, a large area is imaged rapidly with WFM, and specific regions of interest are imaged at high-resolution with TPM. The current implementation of this site-selective tissue cytometry uses a standard, lower speed TPM. While it is sufficient for many site selective studies, it is not suitable for whole organ imaging where higher data acquisition speed is needed. There is potential for a similar site selective scheme to be implemented with video rate TPM (Bahlmann *et al.* 2007; Kim *et al.* 2007*a*,*b*; Ragan *et al.* 2007) providing even greater throughput. Using a video-rate (30 frames s^{-1}) TPM imaging would decrease the imaging acquisition time by 210 times reducing the total acquisition time to merely minutes per specimen.

Although, powerful in its present implementation, it may be desirable in the future to make the imaging process more automated. For example, the results from WFM imaging can be more rapidly and objectively evaluated using automated imaging processing. More specifically, all regions of interest in the WFM image can be segmented and identified automatically. In addition, the centroids of these regions can be computed and compiled into a list. From this list of the positions of interest in the wide field image, appropriate x–y coordinates can be calculated and fed to a robotic x–y positioning stage to provide automatic guidance for high-resolution TPM imaging at the selected sites.

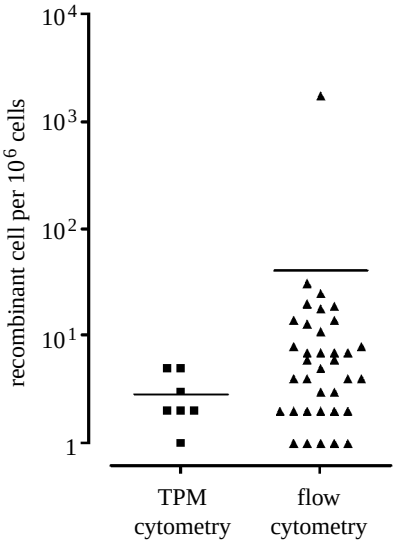

Figure 11. Frequency of recombinant cells in the pancreas tissue. Frequency of recombinant cells per million as determined by flow cytometry ($n=36$), and TPM site-selective tissue cytometry ($n=7$) for juvenile.

In conclusion, we have described a novel imaging platform that provides new avenues for in depth analysis of nuclear, cell and tissue morphometry. In this example, we examined rare fluorescent recombinant cells, but there are many potential applications for this new imaging platform. For example, there is a great interest in being able to track and monitor the behaviour of stem cells used in regenerative medicine. This platform provides a novel and rapid methodology for assessing the location and the morphology of such rare cells.

We thank the Massachusetts Institute of Technology Department of Mechanical Engineering and Biological engineering for their assistance, Dr Seok Chung for assistance in drawings. This work was primarily supported by the NIH

grant R33-CA112151. This work was partly supported by the Singapore–Massachusetts Institute of Technology Alliance. D.M.W.-B. was supported by the National Institute of Health grant T32 ES007020. We thank the Center for Environmental Health Sciences (P30-ES001209-26A1).

REFERENCES

Al-Kofahi, Y., Dowell-Mesfin, N., Pace, C., Shain, W., Turner, J. N. & Roysam, B. 2008 Improved detection of branching points in algorithms for automated neuron tracing from 3D confocal images. *Cytometry A* **73**, 36–43.

Bahlmann, K., So, P. T. C., Kirber, M., Reich, R., Kosicki, B., McGonagle, W. & Bellve, K. 2007 Multifocal multiphoton microscopy (MMM) at a frame rate beyond 600 Hz. *Opt. Express* **15**, 10 991–10 998. (doi:10.1364/OE.15.010991)

Bjornsson, C. S., Lin, G., Al-Kofahi, Y., Narayanaswamy, A., Smith, K. L., Shain, W. & Roysam, B. 2008 Associative image analysis: a method for automated quantification of 3D multi-parameter images of brain tissue. *J. Neurosci. Methods* **170**, 165–178.

Buehler, C., Kim, K. H., Greuter, U., Schlumpf, N. & So, P. T. 2005 Single-photon counting multicolor multiphoton fluorescence microscope. *J. Fluoresc.* **15**, 41–51. (doi:10.1007/s10895-005-0212-z)

Castleman, K. R. 1998 Concepts in imaging and microscopy: color image processing for microscopy. *Biol. Bull.* **194**, 100–107. (doi:10.2307/1543039)

Chen, S. C. & Murphy, R. F. 2006 A graphical model approach to automated classification of protein subcellular location patterns in multi-cell images. *BMC Bioinform.* **7**, 90. (doi:10.1186/1471-2105-7-90)

Denk, W. 1994 Two-photon scanning photochemical microscopy: mapping ligand-gated ion channel distributions. *Proc. Natl Acad. Sci. USA* **91**, 6629–6633. (doi:10.1073/pnas.91.14.6629)

Ecker, R. C. & Steiner, G. E. 2004 Microscopy-based multicolor tissue cytometry at the single-cell level. *Cytometry A* **59**, 182–190. (doi:10.1002/cyto.a.20052)

Gerstner, A. O., Trumpfheller, C., Racz, P., Osmancik, P., Tenner-Racz, K. & Tarnok, A. 2004 Quantitative histology by multicolor slide-based cytometry. *Cytometry A* **59**, 210–219. (doi:10.1002/cyto.a.20054)

Givan, A. L. 2001 Principles of flow cytometry: an overview. *Methods Cell Biol.* **63**, 19–50. (doi:10.1016/s0091-679x(01)63006-1)

Gorczyca, W., Darzynkiewicz, Z. & Melamed, M. R. 1997 Laser scanning cytometry in pathology of solid tumors. A review. *Acta Cytol.* **41**, 98–108.

Helmchen, F. & Denk, W. 2005 Deep tissue two-photon microscopy. *Nat. Methods* **2**, 932–940. (doi:10.1038/nmeth818)

Hendricks, J. B. 2001 Quantitative histology by laser scanning cytometry. *J. Histotechnol.* **24**, 59–62.

Hendricks, C. A., Almeida, K. H., Stitt, M. S., Jonnalagadda, V. S., Rugo, R. E., Kerrison, G. F. & Engelward, B. P. 2003 Spontaneous mitotic homologous recombination at an enhanced yellow fluorescent protein (EYFP) cDNA direct repeat in transgenic mice. *Proc. Natl Acad. Sci. USA* **100**, 6325–6330. (doi:10.1073/pnas.1232231100)

Hwa, A. J., Fry, R. C., Sivaraman, A., So, P. T., Samson, L. D., Stolz, D. B. & Griffith, L. G. 2007 Rat liver sinusoidal endothelial cells survive without exogenous VEGF in 3D perfused co-cultures with hepatocytes. *FASEB J.* **21**, 2564–2579. (doi:10.1096/fj.06-7473com)

Kamentsky, L. A. 2001 Laser scanning cytometry. *Methods Cell Biol.* **63**, 51–87. (doi:10.1016/s0091-679x(01)63007-3)

Kamentsky, L. A. & Kamentsky, L. D. 1991 Microscope-based multiparameter laser scanning cytometer yielding data comparable to flow cytometry data. *Cytometry* **12**, 381–387. (doi:10.1002/cyto.990120502)

Kamentsky, L. A. & Melamed, M. R. 1967 Spectrophotometric cell sorter. *Science* **156**, 1364–1365. (doi:10.1126/science.156.3780.1364)

Kamentsky, L. A., Burger, D. E., Gershman, R. J., Kamentsky, L. D. & Luther, E. 1997 Slide-based laser scanning cytometry. *Acta Cytol.* **41**, 123–143.

Kim, K. H., Buehler, C., Bahlmann, K., Ragan, T., Lee, W. C. A., Nedivi, E., Heffer, E. L., Fantini, S. & So, P. T. C. 2007*a* Multifocal multiphoton microscopy based on multianode photomultiplier tubes. *Opt. Express* **15**, 11 658–11 678. (doi:10.1364/OE.15.011658)

Kim, K. H. *et al.* 2007*b* Three-dimensional tissue cytometer based on high-speed multiphoton microscopy. *Cytometry A* **71**, 991–1002.

Lang, P., Yeow, K., Nichols, A. & Scheer, A. 2006 Cellular imaging in drug discovery. *Nat. Rev. Drug Discov.* **5**, 343–356. (doi:10.1038/nrd2008)

Loo, L. H., Wu, L. F. & Altschuler, S. J. 2007 Image-based multivariate profiling of drug responses from single cells. *Nat. Methods* **4**, 445–453.

Melamed, M. R. 2001 A brief history of flow cytometry and sorting. *Methods Cell Biol.* **63**, 3–17. (doi:10.1016/s0091-679x(01)63005-x)

Perlman, Z. E., Slack, M. D., Feng, Y., Mitchison, T. J., Wu, L. F. & Altschuler, S. J. 2004 Multidimensional drug profiling by automated microscopy. *Science* **306**, 1194–1198. (doi:10.1126/science.1100709)

Powers, M. J. *et al.* 2002 A microfabricated array bioreactor for perfused 3D liver culture. *Biotechnol. Bioeng.* **78**, 257–269. (doi:10.1002/bit.10143)

Ragan, T., Sylvan, J. D., Kim, K. H., Huang, H., Bahlmann, K., Lee, R. T. & So, P. T. 2007 High-resolution whole organ imaging using two-photon tissue cytometry. *J. Biomed. Opt.* **12**, 014 015. (doi:10.1117/1.2435626)

Rieseberg, M., Kasper, C., Reardon, K. F. & Scheper, T. 2001 Flow cytometry in biotechnology. *Appl. Microbiol. Biotechnol.* **56**, 350–360. (doi:10.1007/s002530100673)

Siegel, S. 1956 *Nonparametric statistics for the behavioral sciences McGraw-Hill Series in Psychology.* New York, NY: McGraw-Hill.

Taga, R., Bispo, L. B., Bordin, R. A. & Hassunuma, R. M. 1998 Morphometric and allometric study of the mouse exocrine pancreas growth during the postnatal life. *Okajimas Folia Anat. Jpn* **74**, 271–278.

Tarnok, A. & Gerstner, A. O. 2002 Clinical applications of laser scanning cytometry. *Cytometry* **50**, 133–143. (doi:10.1002/cyto.10099)

Van Dilla, M. A., Trujillo, T. T., Mullaney, P. F. & Coulter, J. R. 1969 Cell microfluorometry: a method for rapid fluorescence measurement. *Science* **163**, 1213–1214. (doi:10.1126/science.163.3872.1213)

Wiktor-Brown, D. M., Hendricks, C. A., Olipitz, W. & Engelward, B. P. 2006 Age-dependent accumulation of recombinant cells in the mouse pancreas revealed by *in situ* fluorescence imaging. *Proc. Natl Acad. Sci. USA* **103**, 11 862–11 867. (doi:10.1073/pnas.0604943103)

Wiktor-Brown, D. M., Kwon, H. S., Nam, Y. S., So, P. T. & Engelward, B. P. 2008 Integrated one- and two-photon imaging platform reveals clonal expansion as a major driver of mutation load. *Proc. Natl Acad. Sci. USA* **105**, 10 314–10 319. (doi:10.1073/pnas.0804346105)